Background simulations for the ATHENA X-IFU instrument: impact on the instrumental design

S. Lotti [a], C. Macculi[a], D. Cea [a], T. Mineo[b], E. Perinati[c], L. Natalucci[a], and L. Piro[a]

[a] INAF-IAPS Roma, Via fosso del cavaliere 100, Rome 00133, Italy;
[b] INAF-IASF Palermo, Via Ugo la Malfa 153, Palermo 90146, Italy;
[c] IAAT - Institute fur Astronomie und Astrophysik, Universitat Tubingen, 72076, Germany

ABSTRACT

On 28 november 2013 ESA selected "The Hot and Energetic Universe" as the scientific theme for a large mission to be flown in 2028 in the second lagrangian point, and ATHENA is the mission that will address this science topic. It will carry on board the X-ray Integral Field Unit (X-IFU), a 3840 pixel array based on TES (Transition Edge Sensor) microcalorimeters providing high resolution spectroscopy (2.5 eV @ 6 keV) in the 0.3-12 keV range. Among X-IFU goals there is the detection and characterization of high redshift AGNs, Clusters of galaxies and their outskirts, and the elusive Warm Hot Intergalactic Medium (WHIM), so great care must be paid to the reduction of the background level. These scientific objectives will be reached if the particle background is kept lower than 0.05 $cts\ cm^{-2}\ s^{-1}$, and to this aim, it is mandatory the use of a Cryogenic AC (CryoAC), as well as an optimized design of the cryostat and of the structures surrounding X-IFU. Our team, that is responsible for the ACD design, performed a detailed study to predict the rejection efficiency of the ACD as a function of its geometrical parameters and design choices. Since no experimental data on the background experienced by X-Ray microcalorimeters in the L2 orbit are available at the moment, the particle background levels have been calculated by means of Monte Carlo simulations using the Geant4 software.

Keywords: ATHENA, X-IFU, X-Ray background, Anti Coincidence Detector, Geant4

1. INTRODUCTION

On 28 November 2013 "The hot and energetic Universe" science theme was selected for the second L-class mission in the ESA Cosmic Vision science program, to be pursued with an advanced X-ray observatory. This mission, whose launch is foreseen in 2028, will address two key questions: how does ordinary matter assemble into the large scale structures that we see today, and how do black holes grow and shape the Universe. The favored candidate to answer these question is the *ATHENA* observatory class mission concept, that has been presented for the ESA call in 2014. *ATHENA* will be placed in orbit at L2, around the second Lagrangian point of the Sun-Earth system in a large halo orbit, with a semi-major axis amplitude of about 700000 km and a period of approximately 180 days. The mission includes two focal plane detectors: a Wide Field Imager (WFI - see Ref. 1), and the one we will deal with in this paper: the X-ray Integral Field Unit (X-IFU).

X-IFU is an array of 3840 Transition Edge Sensors (TES) 250 μm side, composed of Ti/Au sensors and 1 μm Cu and 4 μm Bi absorbers that operates at cryogenic temperatures to achieve the high spectral resolution of 2.5 eV at 6 keV (see Ref. 2).

For any satellite operating in the X-ray band the background is composed of an internal particle component and a diffuse component. The former is generated by particles traveling through the spacecraft, releasing energy inside the detector, also creating swarms of secondary particles (mostly electrons) along the way. These secondaries too can reach the detector, and their flux is often anything but negligible in the soft X-ray band since it is hard to discriminate them using anticoincidence systems (see Ref. 3). This can be an issue especially for "naked" devices such as microcalorimeters or Back Illuminated CCDs, that do not present an inactive layer on the surface capable of absorbing such low energy particles (see Ref. 4). The internal component is estimated and characterized by means of Monte Carlo simulations using the *Geant 4.9.4 p03* software. The latter component is the Soft X-Ray Background (SXRB): a diffuse X-Ray emission observed in every direction. Such a component is modeled using *XSPEC - version 12.8.0* as reported in Ref. 5 and described in Ref. 6.

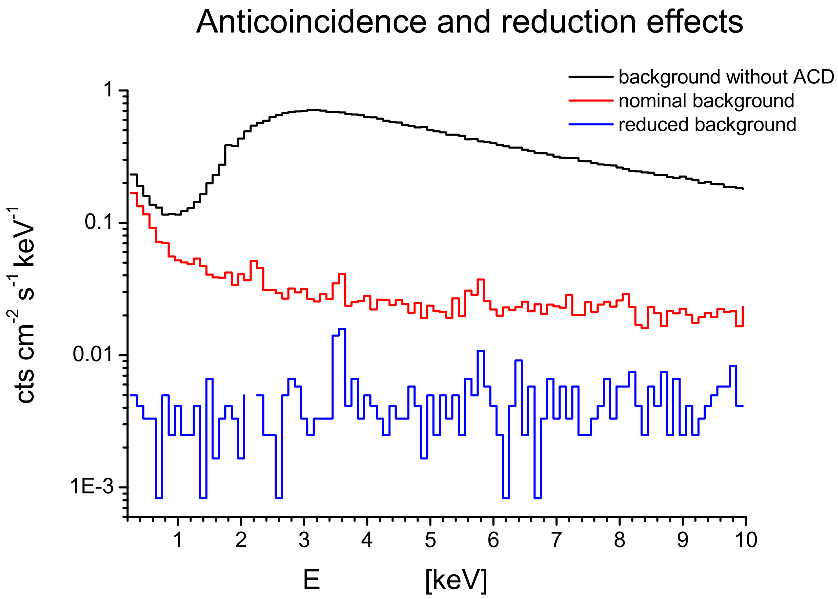

Figure 1. Spectra (100 eV bins) of the background expected on X-IFU in several cases. The black line is the expected background without an anti-coincidence system, the red line is the level expected with an ACD, and the blue line is the official background level.

In this paper we describe the state of the art of the particle background simulations for the X-IFU instrument, and the preliminary simulations made to asses the impact of the Anti Coincidence Detector design on the background level.

2. STATE OF THE ART

There are no experimental data about the Non X-Ray Background (NXB) level experienced by X-ray microcalorimeters in L2, and since *ATHENA* will be the first X-ray large mission placed there, we estimate the NXB with detailed Monte Carlo simulations using the *Geant 4.9.4* software. The first background estimates have been extensively discussed in Ref. 3. Summarizing, as shown in Figure 1, without an Anti Coincidence Detector (ACD) the detector would experience a particle background level of 3.1 cts $cm^{-2}s^{-1}$ in the 0.2-10 keV energy band, mainly induced by primary protons (80% of the total background). The insertion of the ACD (and secondarily the use of pattern recognition algorithms) drops the background by an order of magnitude, to a level of 0.31 cts $cm^{-2}s^{-1}$, cutting the primary protons component and leaving a residual background rate induced mostly by secondary electrons. We refer to this background count rate as the "nominal" background value, since it was obtained in the official configuration foreseen for *ATHENA* before the mission rescope (see Ref. 3). This performance is possible thanks to a solution developed by our team, that is the adoption of an active cryogenic ACD (see Ref. 7,8, and Refs. therein) to be placed underneath (~mm) the X-IFU main detector. It is a cryogenic microcalorimeter constituted by a 2×2 pixel array made of large area Silicon absorbers sensed by Ir TES (Transition Edge Sensor). The main requirements of this ACD that we identified are: a size of at least 18×18 mm^2 (divided among four identical pixel, each 80 mm^2) in order to have sufficient geometrical rejection efficiency, a pulse rise time (which is used for the veto signal) lower or equal to the one of the main detector, (30 μs), and a low energy threshold for the detection of background particles of 20 keV. Prototypes with performance close or within the requirements have already been produced (see Ref. 7, 8).

Since the nominal background level was still higher than the original scientific requirement of the IXO mission (0.2 cts $cm^{-2}s^{-1}$) we searched for solutions to reduce the secondary electrons component, that constituted 85% of the unrejected background and are mainly created in the internal niobium shield. These solutions are reported

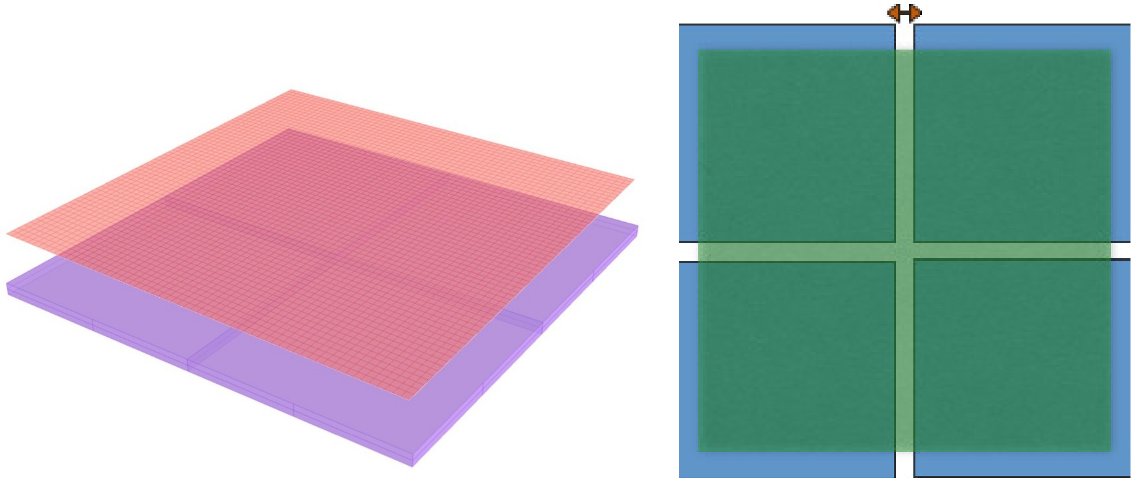

Figure 2. The standard ACD geometrical configuration: in red the main detector and below, in blue, the 4 ACD pixels. On the right a view from the top that highlights the gap among the ACD pixels.

in Ref. 6 and allow to cut the background by another factor of 6 (~83%), bringing us to the unrejected background level of 0.05 cts $cm^{-2}s^{-1}$, which is the current requirement for *ATHENA*. We refer to this value as the "reduced background". This background is the official background level adopted for *ATHENA*, and is available from http://www.the-athena-x-ray-observatory.eu/. All the background spectra considered so far are reported in Figure 1.

All the above estimates have been produced using the Focal Plane Assembly (FPA) foreseen for IXO (see Ref. 3,6). The FPA for *ATHENA*, in fact, has not been developed yet, and the final design will be influenced by the results of our simulations tests. In order to develop the new FPA for X-IFU, as a first step, we run a series of simulation tests to investigate the influence of the size, shape and placement of the ACD. Moreover, different electrons shielding materials and/or configurations have been checked.

3. SIMULATION TESTS

In this section we will illustrate the simulations made to assess the geometry of the ACD and of the electrons shield. Since the simulations performed with the detailed geometrical model are extremely time consuming most of the tests have been conducted on a simplified geometrical model. This model consists of an Al sphere that surrounds the detector blocking protons up to ~120 MeV, the supports, the main detector and the ACD*. Since the setup influences the outcome of the simulations (see Ref. 3) the results obtained with this simplified geometry are to be taken only in relation to each other and not as absolute values. A detailed geometrical model (described in Ref. 3) was used to obtain the results described in Sec. 3.3 and Sec. 3.4.

3.1 Background cross

As stated in Sec. 2 the ACD will be composed of four large area pixels (see Fig. 2) placed underneath the main detector. Due to the presence of a small gap among the ACD pixels it is possible that the background particles will slip through it, and the pixels of the main detector above the gap will experience an higher background respect to the other zones of the detector. There will be then a "background cross" on the main detector, in the center of its FoV, and the emersion of this feature will depend on the size of the gap and the length of the observation. Given the sizes of the gap (10-50 μm) and of the pixels of the main detector (250 μm) the area of the detector that will experience this cross of enhanced background will be 1 or 2 pixel wide, depending on the respective position of the gap and the pixel grid. We took into account three cases: the worst case of a 50 μm gap, the current baseline of a 20 μm gap, the goal of a 10 μm gap, and the ideal case of no gap between the pixels. The 50 μm case results are reported for comparison alongside the no gap case in Fig. 3.

*The sizes, placements and specifications of this simplified model are the ones currently available for *X-IFU*

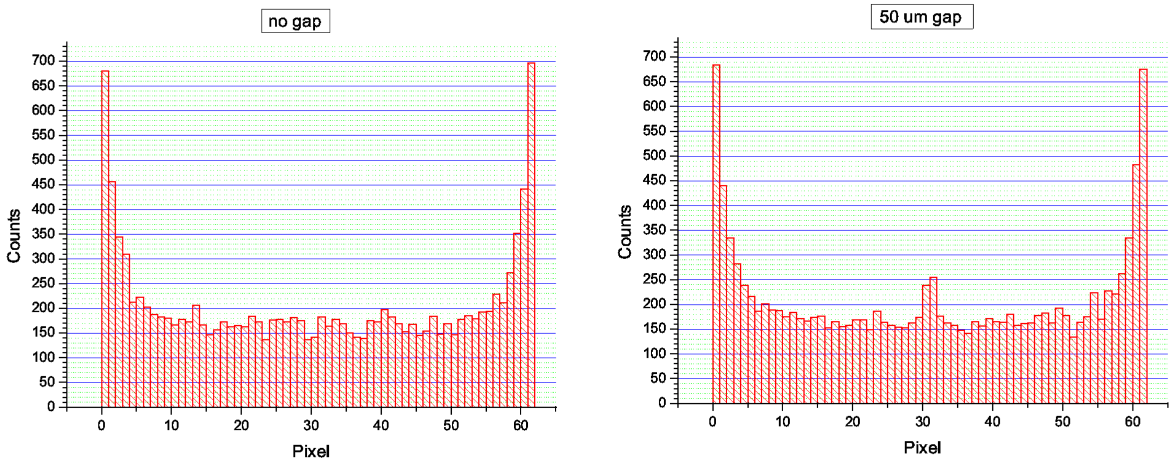

Figure 3. The distribution of unrejected background events among the pixels of the detector, in the ideal case of no gap between the ACD pixels (left), and in the worst case of a 50 μm gap (right). There is a significative increase of background in the central pixels, above the ACD gap.

The first thing to notice is that the total background on the whole detector does not depend on the gap size. In fact increasing the gap only moves unrejected events from the external part of the detectors to its center. But how much the background increases in a pixel of the central line respect to its neighbors? We found that:

- 50 μm gap case: there is an increase of ~50% in the pixels above the cross respect to their neighbors.
- 20 μm gap case: there is an increase of ~22% in the pixels above the cross respect to their neighbors.
- 10 μm gap case: there is an increase of ~9.5% in the pixels above the cross respect to their neighbors.

So there is an increment of the particle background above the gap cross that will become significant, given observations long enough. This increased background will also have a different spectrum since it is composed of particles that are discriminated elsewhere in the detector.

To compute the observing duration affected by the background cross we need to compare the background per unit area from inside to outside the cross, and check if there is a statistically significant difference in a time t. If we label b the background flux outside the cross, A the detector area outside the cross, and b' and A' the corresponding quantities inside the cross we can write the condition to observe the cross with n_σ confidence level as:

b't-bt>n$_\sigma \sqrt{\frac{b't}{A'} + \frac{bt}{A}}$, (1)

with b and b' in $cts\ cm^{-2}\ s^{-1}$ and $b' = b + kb$, and from which we find

$$t > \frac{n_\sigma^2}{k^2 b^2}\left(\frac{b'}{A'} + \frac{b}{A}\right) \quad (2)$$

for X-IFU we have $A' = 7.75 \times 10^{-2}\ cm^2$, $A = 2.325\ cm^2$. In the worst case of 50 μm gap we have $k = 0.5$, and $b_{[3-10\ keV]}{}^\dagger = 0.032\ cts\ cm^{-2}\ s^{-1}$, for $n_\sigma = 5$ we have that $t > 60\ ks$ is needed to detect the enhanced

†The particle background becomes dominant above 3 keV respect to the diffuse emission (see Ref. 6)

Figure 4. An alternative ACD configuration, with the four pixels placed at two different distances from the main detector (a). This way the only gap left is the small square gap in the center (b). On the right the unrejected events distribution for this configuration: it is evident the background disparity in the zones above the four ACD pixels (c).

background cross. So the increment of the background will be noticeable in the typical observation, how much will it affect the observations?

If we assume the worst case of a source located in the center of the detector, the background increment depends on the extraction region: point sources can have a background up to 50% higher, depending on the fraction of the extraction region placed on the cross, while for extended sources it is less influent as the extraction area increases. This enhanced background on the detector can not be subtracted properly in a single observation, since the area of the cross is too small to get a sufficient sampling ($A' \times b' = 3.7\ cts/ks$, that for a 100 ks observation gives ~400 cts).

In conclusion the safest approach is to use dithering during the satellite pointings, or at least avoid to place the target source in the detector center. If this is not possible in we should take into account the difference in the particle backgrounds inside and outside the cross. A possible strategy can be to put together several observations to find the ratio of the two backgrounds as a function of energy $R(E) = b'(E)/b(E)$, and use $b(E)\,R(E)$ as background to be subtracted from the pixels on the cross.

Two levels ACD

An alternative ACD configuration foresaw four rectangular pixels on two different planes, slightly overlapping and leaving a small square gap in the center ($50 \times 50\ \mu\text{m}^2$) (see Fig. 4a,b). This way there is no significative gap between the four pixels of the ACD. The problem with this configuration is that the more the ACD is close to the main detector and more efficient it is (see Ref. 6), so with this solution we have four background zones in the detector (see Fig. 4c), with the two nearest pixels of the main detector exhibiting a background 40% lower (20% lower in the central zone) respect to the other two pixels. This is particularly noxious for extended sources that can end up in different background zones. This configuration is therefore less preferable.

Seven-pixels ACD

Another possible solution is to have a central ACD pixel surrounded by 4 or 6 rectangular pixels (see Fig. 5). This way the total background on the detector remains the same, but the increased background that previously manifested as a cross in the detector center is moved to the detector outer zones. This configuration however places some problems, such as the need to redesign the ACD support in order to sustain the central pixel and link it to the thermal bath. This solution will be investigated in the next future to check its feasibility.

3.2 ACD Size

We run a series of simulations to assess the optimal ACD size and placement according to the manufacturing possibilities and to the gain in background reduction efficiency. The baseline for this study are the official X-IFU specifications: a main detector of $15.5 \times 15.5\ mm^2$, and an ACD of $18 \times 18\ mm^2$, placed 1 mm below the main detector.

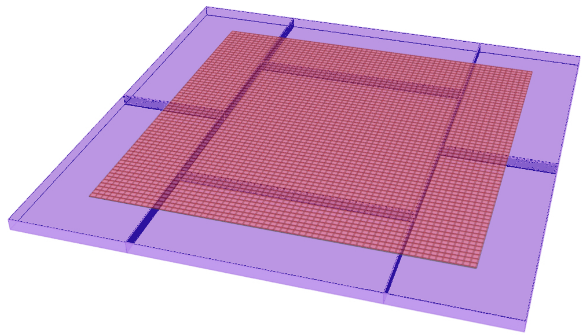

Figure 5. An alternative approach that foresees a central ACD pixel surrounded by six (or four) rectangular pixels.

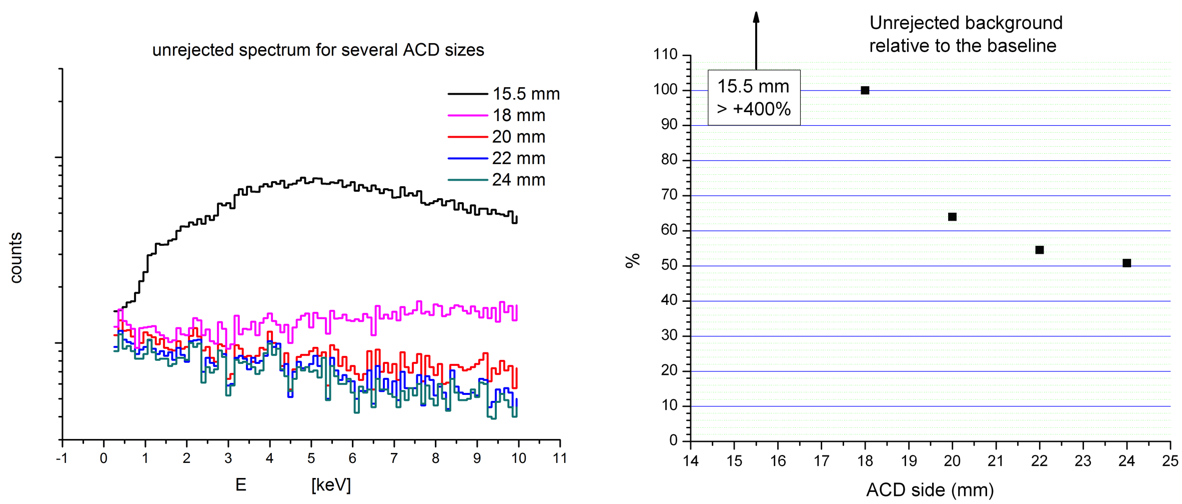

Figure 6. The spectra of the unrejected background on the whole detector for different ACD sizes (left), and the ratio of these different backgrounds to the background of the official configuration.

Sizes. We first investigated the rejection efficiency of the ACD as a function of its size, starting from an ACD with the same size of the main detector, and increasing its size until it reached a size of $24 \times 24\ mm^2$, that is the current manufacturing limit. The results are reported in Fig. 6.

As we increase the size of the ACD we can see that its efficiency in rejecting the particles increases. The decrease in background is not uniform both in energy and in the different detector zones: in fact what we are discriminating with increasing efficiency is the high energy component of the background, that is induced by high energy particles with skew trajectories that cross the detector but not the ACD, and this happens more easily when they hit the detector near its edge. Increasing the ACD size increases the fraction of those that intercept the ACD as well, and therefore its geometrical efficiency.

A confirm of this interpretation can be found in Fig. 7, where we plot the background in the central zone of the detector[‡] as function of the ACD size. From the plot we can see that the background in the detector center is not dependent on the ACD size, and this confirms that the difference in the rejection efficiency concerns the outer zones of the detector. The effect is particularly enhanced when the ACD has the same size of the main detector (see Fig. 6a): in this case roughly 50% of the high energy particles (mostly primary protons) can cross

[‡]We define the central zone excluding the outer 10 pixels on each side of the main detector.

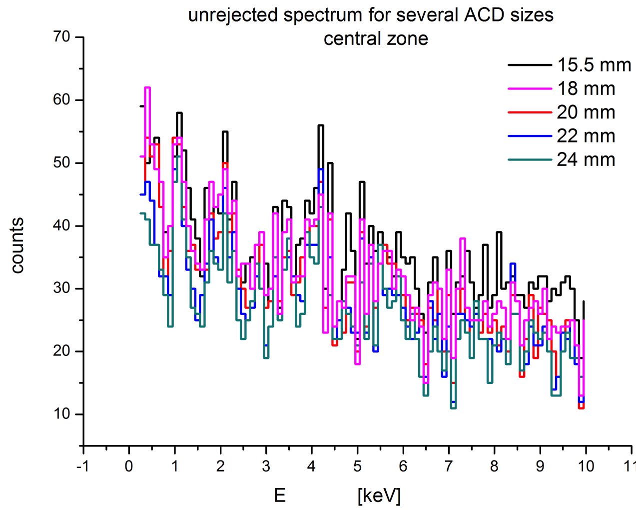

Figure 7. The spectra of the unrejected background in the central zone of the detector[§] for different ACD sizes.

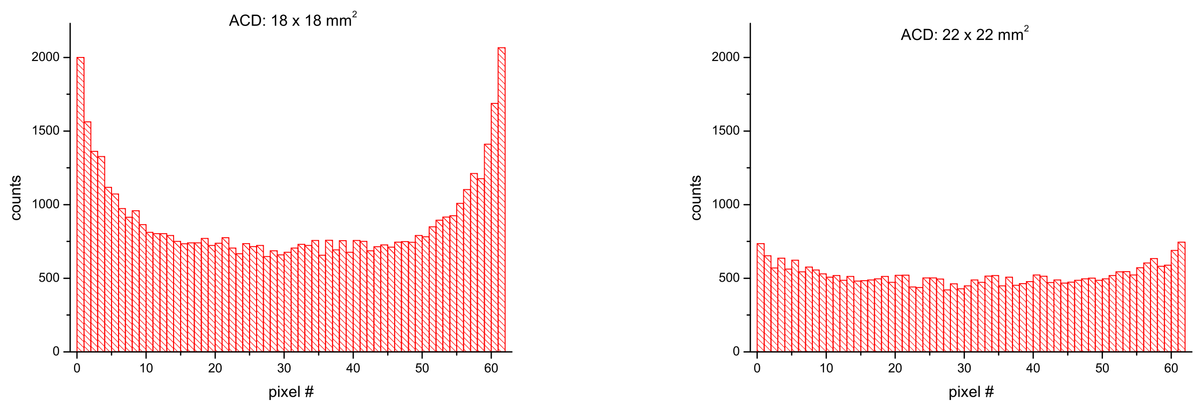

Figure 8. The distribution of counts on the detector in the case of an ACD of 18×18 mm^2 (left), and in the case of a 22×22 mm^2 ACD (right).

the detector without being vetoed, and therefore the background spectral shape resembles what we would have obtained without an ACD, that is the Landau distribution generated by MIP particles crossing a thin layer.

If we plot the efficiency of each setup relative to the nominal configuration (Fig. 6b) we can see that increasing the size of each ACD pixel by 1 mm respect to the baseline we can cut 35% of the background, and further increasing the size allows to reduce the background by a factor two respect to the nominal configuration. The effectiveness of enlarging the ACD decreases with its size since the incidence angle of a particle to not intercept the ACD goes as $atan\left(\frac{d}{x}\right)$, where d is the distance between the two detectors and x is the size of the ACD that exceeds the main detector size. So a certain tradeoff that takes into account also manufacturing problems for large absorbers has to be found.

Besides reducing the background on the detector, enlarging the ACD has also the advantage of uniforming the background across the whole detector (see Figure 8). This can be of great importance since the outer zones of the detector (i.e., the zones outside the FoV) will likely be used for the particle background characterization.

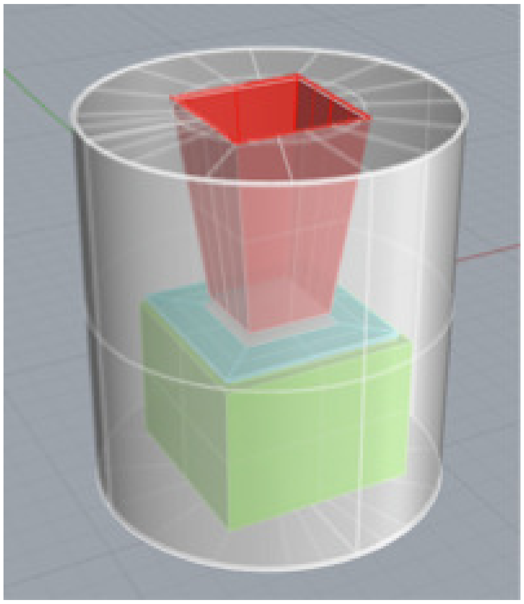

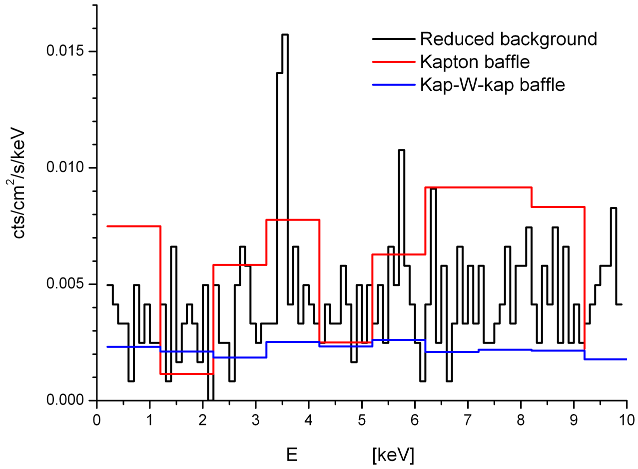

Figure 9. The geometrical configuration of the internal zone of the cryostat (see also Figure 10a) with the kapton baffle in red (right), and on the right the spectrum obtained with this geometry (the red line) compared to the official one (black).

3.3 Electron baffle

The most effective solution identified in Ref. 6 (covering the whole Nb shield in kapton) despite being able to reduce the background down to the official level could place some manufacturing problems. An alternative approach is to place the kapton closer to the detector, in the shape of a baffle between the Nb shield and the detector (see Figure 9a). The baffle coverage is not complete, and the background obtained is slightly higher in the baffled configuration ($5.5 \times 10^{-2}\ cts\ cm^{-2}\ s^{-1}$) than in the official configuration ($4.7 \times 10^{-2}\ cts\ cm^{-2}\ s^{-1}$) (see Figure 9b).

Materials.

To optimize the shielding materials of which the baffle is composed a multilayer that alternates high and low density materials is the best choice (see Ref. 9). As a first test we added a 250 μm tungsten layer inside the kapton and repeated the simulation with this kapton-tungsten-kapton multilayered baffle. Tungsten is in principle a suitable material for cryogenic space applications because of its low transition temperature (15 mK), but the technical feasibility of such a structure is yet to be discussed. The results of this simulations are reported in Figure 9 along with the background obtained with the simple kapton baffle and the baseline "reduced" background.

In this configuration the background decreases by a factor of two respect to the official configuration, and reaches a value of $2.1 \times 10^{-2}\ cts\ cm^{-2}\ s^{-1}$.

3.4 Enveloping ACD

As a last test we simulated the insertion of an ACD that completely surrounds the main detector on its sides (see Figure 10a), effectively shielding the detector from the electrons generated in the cryostat. This setup is quite unrealistic, and its purpose is to assess the lowest background achievable for X-IFU, understand how much we are far from this level and if it is worthwhile to invest in implementing such a solution.

What we found from the simulation is that in such setup the background is reduced by a factor of ~6 down to the level of $7 \times 10^{-3}\ cts\ cm^{-2}\ s^{-1}$ (see Figure 10b). This background is induced mainly by photons (83%), either through the absorption of the Bi K fluorescences at ~16.5 keV that are then reemitted as Bi L fluorescences

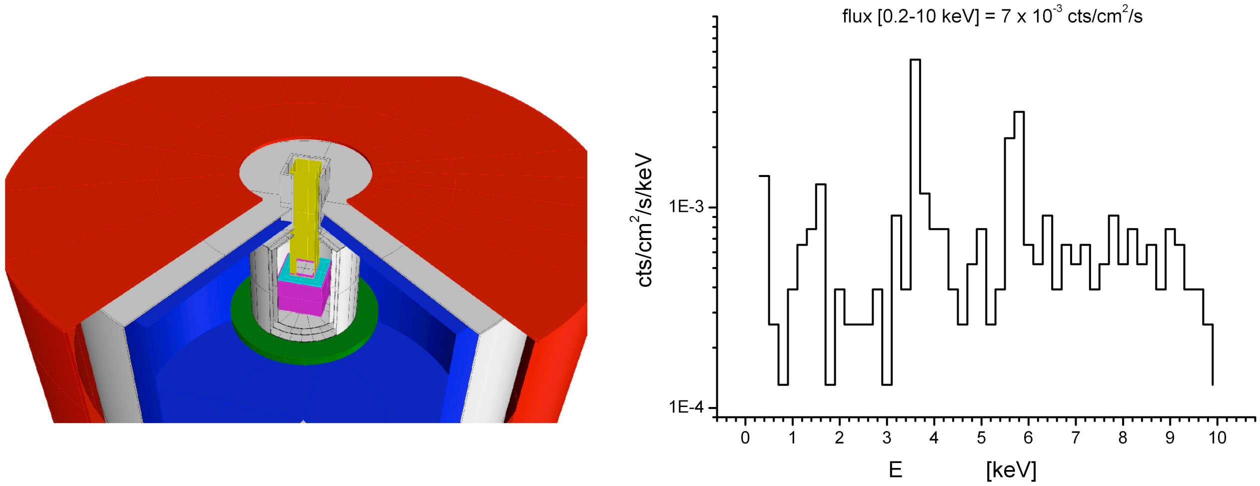

Figure 10. The geometry of the cryostat, with the enveloping ACD highlighted in yellow (left), and the spectrum obtained with this configuration (right).

(10.8-15.2 keV), leaving in the detector an energy inside its sensitivity range, or through Compton scattering of high energy photons that deposit a small fraction of their energy.

The electron component is greatly reduced by this setup, and now represents less than 3% of the unrejected background, and the reason for this is quite simple: since the ACD is the last surface seen by the detector the secondary electrons either are generated outside it (and therefore are blocked/detected by it), or they are generated inside the ACD by the passage primary particles (and in this case is the primary particle that triggers the ACD). Either way they are discriminated, and the only electrons that are able to reach the detector are the ones coming from the small space between the main detector and the ACD (the one placed below the main detector), or the ones created in the supports.

This background level, being composed mainly of fluorescence photons, could be further reduced through the use of a graded-Z shield. However an accurate estimate of to which extent this solution is feasible that keeps into account benefits and costs has yet to be done.

4. SUMMARY AND CONCLUSIONS

We analyzed the problems placed by the nominal geometrical configuration of the X-IFU instrument, testing several possible solutions, and explored different paths to further reduce the particle background level, improving the efficiency of the anti-coincidence system or reducing the flux of secondary particles towards the detector.

We found that the presence of a gap among the ACD pixel transfers background counts from the edge of the detector to its center, and this can possibly be a problem for observations longer than 60 ks. To avoid this problem two different modifications to the ACD geometry have been tested. In the first alternative setup we had the four pixels of the ACD placed on two different planes, slightly overlapping to leave a small square gap in the center. In the second setup we arranged a central square pixel surrounded by several rectangular ones, simply moving the gap in the external zone of the detector. The first setup revealed a fatal flaw, which is the creation of four different background zones in the detector due to the dependence of the ACD rejection efficiency on the distance from the main detector. The second setup does not have such problem, but its technical feasibility has yet to be investigated. In case that neither of these solutions are feasible we will have to pay attention to this problem, avoiding to place the target source above the gap, using dithering or compensating with ad-hoc analysis techniques.

To assess the optimal size of the ACD detector we simulated several cases on a simplified geometrical model, starting from an ACD with the same size of the main detector, until the current manufacturing limit. We found that increasing the size of each pixel of the the ACD by 1 mm reduces the background of ~40% respect to the

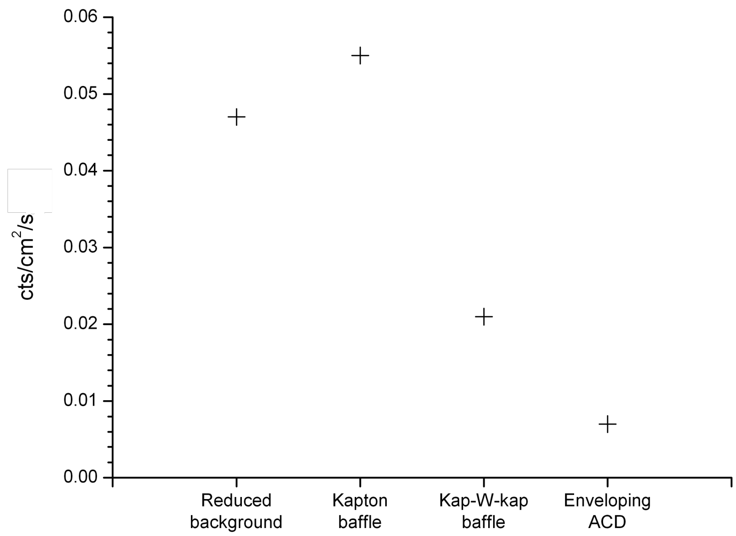

Figure 11. All the background considered in this work.

nominal configuration (four pixels, each 9×9 mm^2), and that the optimal results is obtained with a set of 4 pixels, each 11×11 mm^2, that reduces the unrejected background by a factor of two. This reduction of the unrejected background is concentrated in the external zones of the detector. We also tested the dependence of the background from the distance between the main detector and the ACD, and found that moving the ACD from 1 mm to 0.5 mm reduces the background by 40% (20% in the central zone). This effect does not add linearly to the benefits of enlarging the ACD, since they both exploit the same principle, which is to reduce the angle available for a particle to pass through the main detector without hitting the ACD.

We investigated the effect of moving closer to the detector the kapton layer foreseen inside the cryostat in the original geometry, in the shape of a baffle between the Nb shield and the detector. This has the advantage of not having to cover the whole internal niobium shield in kapton despite being able to reduce the background to the same level, avoiding several manufacturing problems. We also tested the effectiveness of a multilayer of high an low density materials in stopping the electron flux towards the detector, and found that a kapton-tungsten-kapton baffle reduces the background by a factor of two.

As a last test we simulated the insertion of an ACD that completely surrounds the main detector on its sides, to assess the lowest background achievable for X-IFU. We found that this unrealistic setup the electron component is almost completely erased, and the background is reduced by a factor of 6, down to the level of 7×10^{-3} cts cm^{-2} s^{-1}. The remaining background is mainly induced by high energy and fluorescence photons, and could in principle be further reduced with the use of a graded-Z shield.

All the background levels considered in this work are reported in Figure 11 for comparison.

ACKNOWLEDGMENTS

This work was supported by ASI contract I/035/10/0-10-308. We wish to thank Memmo Federici and Bruno Martino for the development of GFORC (see Ref. 10), the computer cluster that allowed the Geant4 simulations in a reasonable time.

REFERENCES

[1] Nandra, K., "The hot and energetic universe," *Athena website: http://www.the-athena-x-ray-observatory.eu/* (2013).

[2] Barret, D., "The x-ray integral field unit (x-ifu) for athena," *Athena website: http://www.the-athena-x-ray-observatory.eu/* (2013).

[3] Lotti, S., "Estimate of the impact of background particles on the x-ray microcalorimeter spectrometer on ixo," *NIMA* **686**, 31–37 (2012).

[4] Lotti, S., [*Performance estimates and design optimization of space based instruments for X-Ray astrophysics*], La Sapienza University (2013).

[5] McCammon, R., "A high spectral resolution observation of the soft x-ray diffuse background with thermal detectors," *The Astrophysical Journal* **576**, 188–203 (2002).

[6] Lotti, S., "The in-orbit background of x-ray microcalorimeters and its effects on the observations," *Astronomy and Astrophysics - accepted for publication on 04/06/2014* (2014).

[7] Macculi, C., "The cryogenic anticoincidence detector for athena-xms: preliminary results from the new prototype.," *Proc. of SPIE* **8443** (2012).

[8] Macculi, C., "The cryogenic anticoincidence detector for athena," *Journal of Low Temperature Physics* **167, Issue 5-6**, 783–794 (2012).

[9] Masti, "Shielding protection of electronic circuits against radiation effects of space high energy particles," *Advances in applied research* **3**, 446–451 (2012).

[10] Federici, M., "Gforc: A fast expendable and cheap computer cluster devoted to geant4," *Astroinformatics* (2011).